Analysis of Supersonic Intake Design for Multi-Row Disk Intake Device Under Varying Mach Numbers and Angle of Attacks

Jayanta Sinha
Research Scholar
Amity Institute of Aerospace Engineering
Amity University Uttar Pradesh, Noida
India

Sanjay Singh
Professor
Amity Institute of Aerospace Engineering
Amity University Uttar Pradesh, Noida
India

Om Prakash
Professor
Department of Aerospace Engineering
University of Petroleum and Energy Studies, Dehradun
India

Dhruv Panchal
Post Graduate Student
Amity Institute of Aerospace Engineering
Amity University Uttar Pradesh, Noida
India

This research investigates the performance of a MRD intake design for supersonic aircraft engines, focusing on its behavior under varying Mach numbers and angles of attack. Utilizing steady-state, two-dimensional RANS simulations with a k-ω SST turbulence model, the study compares the MRD intake to conventional intake designs. The simulations were conducted across a range of Mach numbers from 2.0 to 5.0 at an angle of attack of 0° to 10°. The results reveal that the MRD intake achieves optimal mass capture ratio and total pressure recovery near the design Mach number of 3, significantly outperforming conventional intakes in terms of efficiency and stability. The analysis also highlights the impact of flow separation on intake performance, particularly at low and high Mach numbers. Furthermore, the study explores the effects of varying angles of attack, showing an increase in total pressure recovery up to 6°, after which performance begins to decline. These findings provide valuable insights into the aerodynamic optimization of supersonic intakes, offering potential improvements in the design and operation of high-speed aircraft.

Keywords: *Multi-Row Disk Intake, Supersonic Intake Design, Mach Number, Angle of Attack, Total Pressure Recovery, Mass Capture Ratio, Numerical Simulation.*

1. INTRODUCTION

The design and optimization of air intake systems are critical for the performance of high-speed aircraft engines, particularly those operating under supersonic and hypersonic conditions [1, 2]. Air intake, or intake, is a crucial component in aviation engines that directly influences the efficiency of air capture, flow quality, and overall engine performance [3, 4]. For engines that operate at high speeds, particularly in military aircraft, the air intake design must ensure maximum mass flow rate while minimizing aerodynamic losses to achieve optimal combustion [5, 6].

The complexity of designing supersonic intakes, such as mixed compression intakes, arises from their dual requirement to manage both internal and external compression effectively [7-9]. These intake systems must handle various operational challenges, including backpressure effects, boundary layer interactions, shock waves, and flow separations, all of which can signifi–cantly impact the performance metrics like mass capture ratio and total pressure recovery. Additionally, condi–tions like varying angles of attack, turbulence, and the wake of preceding aircraft [10] can create non-uni–formities in the flow, further complicating the design processes and applications.

Recent studies have investigated the aerodynamic behaviour of mixed compression intakes [11-14] under various conditions. Numerical simulations and expe–rimental analyses have provided insights into pheno–mena such as intake buzz [11], a form of oscillation caused by boundary layer interactions and shock wave reflections. These studies aim to refine intake designs to handle different Mach numbers and operational scenarios more effectively.

The statistical investigations on the intake design was numerically studied by V.M. Krushnarao Kotteda and Sanjay Mittal [15] with various back pressures and their effects. The results showed that as the back pressure increased, the position of normal shocks moved closer to the throat, and the high back pressure turned the performance into the subcritical conditions. Fujii, M. et, al. [16] conducted an experiment to investigate the axisymmetric intake with various angles of attack in order to analyze intake performance at high angle of attack. Their findings indicate that as the angle of attack increases, the performance of the supersonic intake deteriorates, which in turn affects the mass capture ratio and total pressure recovery. Further it highlights that an increase in the angle of attack exacerbates flow distor–tion, resulting in unstable flow patterns inside the intake. This instability can potentially lead to "unstart" conditions where the intake fails to properly function at supersonic speeds. The experimental examination of the buzz phenomenon for the mixed compression super–sonic intake was carried out by Simon Trapier, Philippe Duveau, and Sébastien Deck [17]. Their findings demonstrate the existence of two distinct forms of buzzes. The first one is a loud buzz that causes a

Received: September 2024, Accepted: December 2024
Correspondence to: Mr. Jayanta Sinha, Amity Institute of Aerospace Engineering, Amity University Uttar Pradesh Sector 125, Noida, UP-201313, India
E-mail: jsinha1987@gmail.com
doi: 10.5937/fme2501038S
© Amity University Uttar Pradesh. All rights reserved

decrease in the mass flow rate of the intake, and the second one is a quiet buzz that causes the intake to move into the unstart position . Lee, H.J. and Jeung, S. [18] have conducted both numerical and experimental research, and their findings show that the varied effects of buzz may be seen via the lens of the study of pressure fluctuation. Chaudhary, P.K. [19] performed a numeri–cal research using a variety of back pressures, and the results revealed that an increase in the value of the back pressure ratio led to an input into a subcritical condition. The starting characteristics of a scaled model of a rectangular intake at Mach 3 were explored by D. M. Van Wie et al. [20]. The researchers found that there is a critical backpressure at which the intake transitions from a "started" to an "unstarted" condition. This critical backpressure is highly sensitive to the free-stream Mach number and the geometry of the intake. The findings indicate that careful control of the backpressure and understanding its relationship with Mach number are crucial to maintain the desired performance. Namkoung et al. [21] finds that throttling conditions (i.e., variations in engine power demand or changes in backpressure) also play a critical role in the onset and intensity of intake buzz. Reducing the engine's throat area or increasing backpressure can lead to a condition where the airflow within the intake becomes unstable, resulting in oscillations. Specifically, the study shows that there is a critical range of throttling conditions where buzz is most likely to occur, and this range shifts with changes in the angle of attack. Further experimental work by Yu, K. et al. [22] has characterizes the intake start process under various Mach number conditions. The paper concludes that the rate of change in Mach number (ramp rate) significantly affects the intake start process. Gradual change in Mach number has much desirable effects by avoiding the flow instabilities that leads to unstart of the Air intake. Most significant finding that resonate with the current paper is there their findings that emphasize the need for designing intakes that are capable of handling a wide range of Mach numbers and maintaining stability across different operational conditions. The study recom–mends exploring innovative designs that can dynami–cally adapt to changing flight conditions, thereby reducing the risk of intake unstart and improving overall aircraft performance.

This paper explores the steady-state simulation of a MRD intake at different Mach numbers, examining the effects of varying Angle of attack and flow conditions on the intake's performance. The research utilizes a va–lidated RANS solver with a k-ω SST turbulence model to analyze the intake performance under various scenarios. The findings aim to contribute to the optimization of intake designs for improved performance, particularly at critical Mach numbers and angle of attack.

Through the extensive literature review and research it has been found that significant work has been carried out in the domain of air-intake analysis at different Mach number and the angle of attack for conventional air-intake systems. But limited work has been carried out on integration of the MRDID with the conventional air-intake system and its analysis over the wide range of supersonic Mach number to obtain the optimum performance range. Novelty of the paper lies in the fact that it has analysed and reported the efficiency para–meters like TPR and MCR on an air-intake system where a novel MRDID has been used for intake comp–ression. At the same time the comparison on TPR and MCR have been drawn with respect to the single ramp based conventional air-intake system to find out the effectiveness and improvement that MRDID based air-intake system offers. Detailed design of the conven–tional air-intake design and the novel MRDID based air-intake geometry is shown in figure 1(b) and 1(a) respectively. Details of MRDID and its advantages have been reported by Kobayashi et al. [23, 24] and Sinha et al. [6, 25]. So, far MRDID has been analysed as an isolated device only but in the present paper it has been used along with the conventional air-intake system. Lot of researches are available on the performance analysis of Single ramp, double-ramp and bump compression on the overall air-intake system and subsequent pressure recovery. But the compression capability of novel MRDID device and its impact on overall pressure recovery and the intake efficiency have been reported through this paper. Also, the present work has provided lot of insight into the internal flow development, shock train structure and local flow separations in much detailed and comprehensive manner. Through this paper, the optimization of the Mach number and the optimum angle of attack have also been reported. This research is also significant as in the future it will set the operational limit for the Air-intake system using MRDID for any Supersonic ad Hypersonic Aircraft

The results and discussion of present paper has two parts. In the first part - key performance parameter like TPR and MCR have been obtained for Conventional air-intake system and the modified air-intake system integrated with MRDID at different Mach number. In the second part, the MRDID integrated air intake has been analysed at different angle of attack to obtain the efficient operational range. TPR and MCR has also been plotted to understand the most efficient angle of attack for its operation. The unique contribution of this research is that it presents the internal flow physics, performance parameter characteristics and analysis over a wide range of Mach number ranging from 2 to 5 split into multiple decimal level Mach numbers to have highly optimized results. Back pressure of 7 bar has been kept constant for all the simulations. Angle of attack has been varied from 0° to 10° at the optimum Mach number to obtain the most optimized flight conditions. A new air intake has been designed to suit the MRDID provided by Sinha et al. [25]. Motivation for the design of the air-intake has been taken from the work of Emami and Trexler [26]. It forms the basis of further research and in-house code development to evaluate the performance parameters.

The sole purpose of this paper is to obtain the effect of MRDID on a particular intake and evaluate its performance for different Mach number and angle of attacks and then to define the optimum operation range for the given intake. Unsteady phenomena and buzz have not been covered in this paper as it will make this paper extremely lengthy.

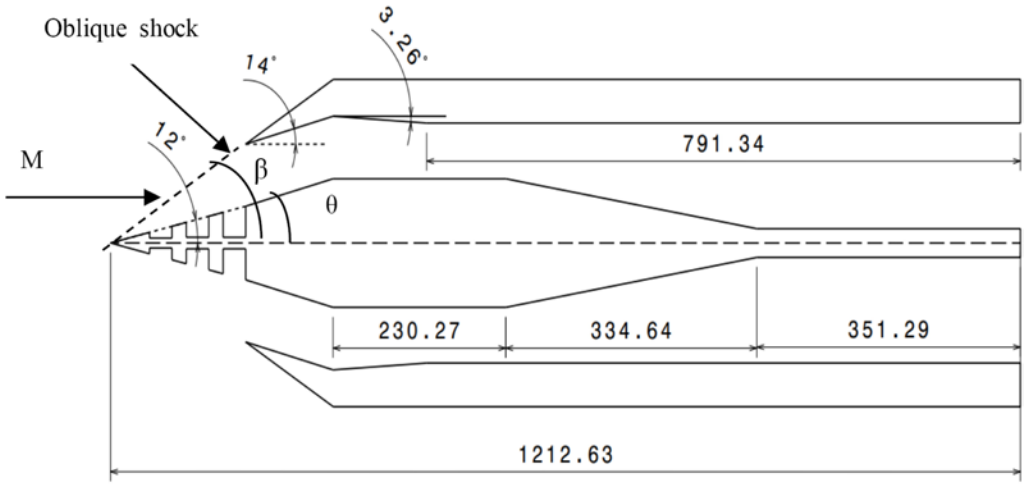

Figure 1(a). Air Intake Geometry modified with MRDID at the front

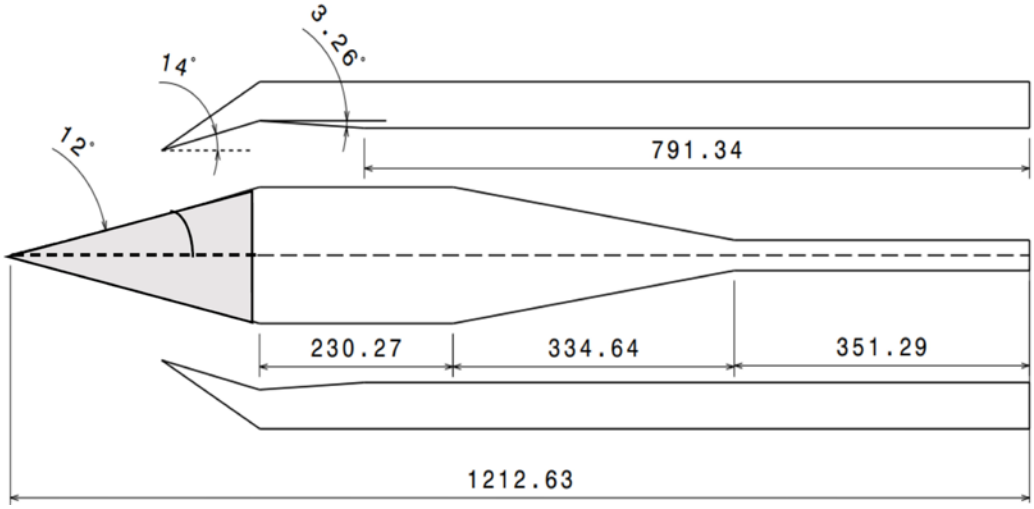

Figure 1(b). Air Intake Geometry with single ramp

2. GEOMETRY DESIGN

The geometry of the intake used for numerical analysis is obtained through multiple iterations based on the literature provided by Emami and Trexler [26]. Air intake geometry is shown in figure 1. The geometry has a mixed compression type of intake with MRDID fitted at the front. Relations between θ- β -M have been used to construct the geometry. The expression relates the free stream Mach number M, the deflection angle θ, and the oblique shock angle β. From the relation, it is obvious that each situation has two possible solutions one with a lower β angle that is referred to as the weak solution and one with a larger angle β that is referred to as the strong solution. We have used weak solution to minimize the loss at the intake.

In order to slow the flow, the convergent type of duct that has been constructed for incoming supersonic flow has been developed. Following the typical shock, the flow will turn subsonic. In order to achieve the combustion process that you wish, subsonic flow is necessary. In light of this, a subsonic intake has also been designed. When taking into account the boundary layer obstruction, the neck area is designed to have larger dimensions than necessary to avoid the blockage of the boundary layer. In order to achieve a higher mass capture ratio, the design was developed in such a way that the first shock will directly interact with the cowl, and the oblique shock that will result from the leading edge of the first cavity will also attach to the cowl. Both of these interactions were planned out in advance.

3. SOLVER SET-UP & GRID GENERATION

For the purpose of carrying out the numerical simu–lations, validated steady state, two-dimensional (2D), implicit Reynolds-averaged Navier-Stokes equations (RANS) solver with a k-ω SST turbulence model has been utilised. The solution methods comprise implicit formulation, Roe-FDS flux scheme, and gradient Green-Gauss cell-based spatial discretization with second-order upwind flow scheme. Complete solver set up data is given in Table 1. The solver is validated by utilising benchmark data that is generated by a closed-form analytical model. This ensures that the solver is accurate. The wall Y+ value set as 1. The quadeleteral shape of the mesh chosen for all presented case, shown in figure 2.

To capture the flow behavior, a large fluid domain has been created and the details about the domain are also shown in figure 2. Total length of the domain is kept twice that of the model length for better shock

capture. Also the height of the domain is kept 4 times the width of the simulation model. Though, multiple iterations have been underatken to optimize the size of the domain for time effective simulations.

Table 1. Solver Set-up

Scheme/Parameters	Type/quantities
Solver precision	Double precision
Solver type	Density-based implicit, steady state
RANS	k-ω SST (2 PDE model)
Inviscid flux scheme	Roe flux-difference splitting scheme
Spatial discretization	Second-order upwind scheme
Gradient evaluation	Least squares cell-based

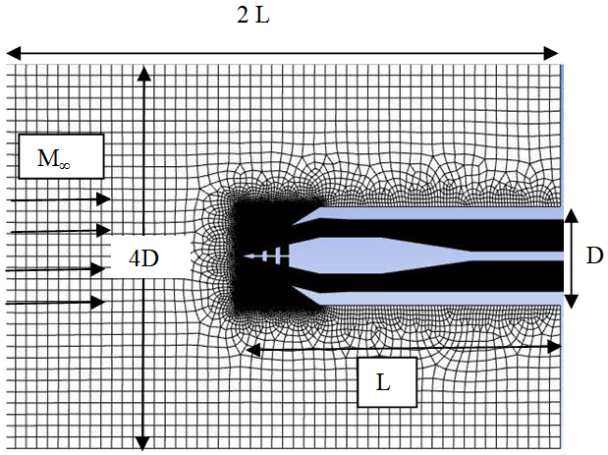

Figure 2. Domain Meshing

The intake and the upper and lower domain boundaries have been specified by pressure far-field boundary condition. The MRDID and the Air intake structure are specified with no-slip wall boundary conditions, and the domain outlet is specified with pressure outlet. Figure 3 provides the enlarged view of the meshing inside the air intake. The grids points are converged near the wall to capture the boundary layer and the shock reflection from the wall accurately.

During the simulation, the residuals of continuity, energy and turbulent kinetic energy were monitored. In addition, the convergence history for drag was also monitored during the entire solution period. Results were analyzed only when it was ascertained that the residuals have converged to the order of 10^{-3}.

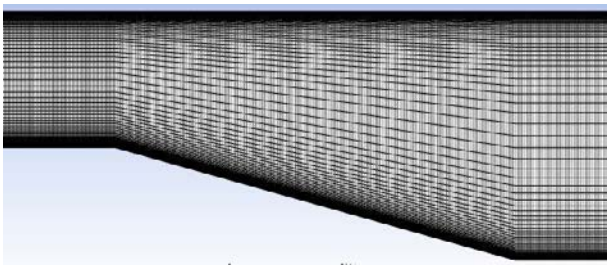

Figure 3. Enlarged view of the internal meshing

4. SOLVER VALIDATION & GRID INDEPENDENCE TEST

The solver is verified using benchmark data from a closed-form analytical model [27-29]. Furthermore, numerical results are validated using benchmark data [23-30] for various operating conditions. Data Presented by Gholap et al. [29] and Tembhurnikar et al. [31] have been specifically used to validate the numerical turbulence model.

Since, no experimental work has been undertaken in support of the present research work, we have validated the work using the published paper by Milicev [32] and Damljanović et al. [33]. The off-design performance of the model in the wind tunnel has been studied based on the work of Damljanović et al. [34]. The validated grid reported by Sinha et al. [6, 25, 35] has been used for the current simulation.

Figure 4 presents the numerical validation undertaken on the air intake model in reference to the experimental data published by Emami and Trexlar [26]

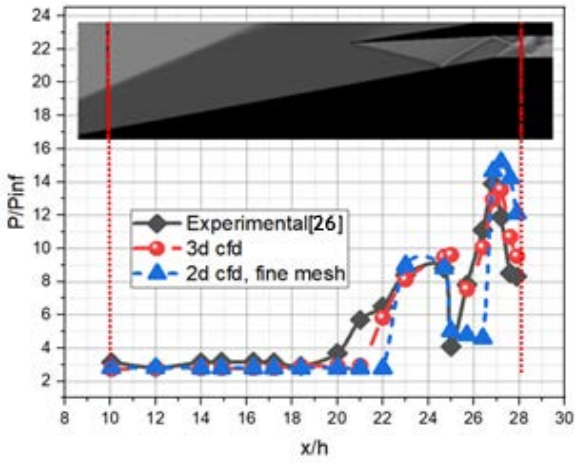

Figure 4. Numerical validation check with reference data

Further validation has been undertaken based on the experimental data reported by Kobayashi et al. [24] on the MRDID. He reported the C_D values on the Type 2 and Type 3 MRD models. Complete details on the Type 2 and Type 3 models can be found in the reference paper. Here C_D value has been validated through the numercial simulation. Two different types of meshing have been used – Coarse mesh and Fine mesh. Coarse mesh has 2,85,000 grid points and the Fine mesh has 5,50,000 grid points. Table 2 and 3 presents the numerical validation undertaken in reference to the experimental data published by Kobayashi et al. [24] and the deviation in the results for both the fine mesh and the coarse mech respectively.

Table 2. Grid validation with Fine mesh

MESH TYPE	**C_D Values**		
FINE MESH	**TYPE 1**	**TYPE 2**	**TYPE 3**
REFERENCE DATA [24]	0.076	0.08764	0.1035
Numerical data	0.07854	0.0863	0.1026
,ERROR%	**3.34**	**1.52**	**0.87**

Table 3. Grid validation with coarse mesh

MESH TYPE	**C_D Values**		
COARSE MESH	**TYPE 1**	**TYPE 2**	**TYPE 3**
REFERENCE DATA [24]	0.076	0.08764	0.1035
Numerical data	0.07878	0.0838	0.1021
ERROR %	**3.658**	**4.38**	**1.35**

Above data shows the close proximity of the Experimental data and the numerical data. However, for the better accuracy we have used Fine Mesh for further simulations. Further details on the experimental models and the simulation models can be obtained in the paper by Sinha et al. [25].

To bring higher level of accuracy in the mesh generation and the solver selection for the internal simulation, we have undergone further computational validation for the mixed compression intake with the simulation data reported by Das and Prasad [36].

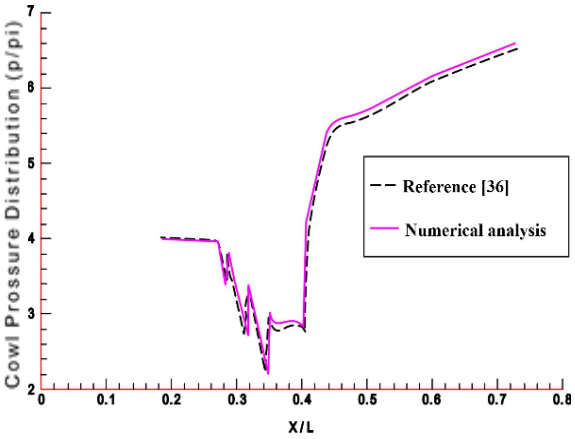

Figure 5. Validation of the Numerical simulation

Static pressure distribution over the ramp and cowl surface of the clean air intake (without MRDID) model at zero degree cowl deflection has been reported by them. Numerical pressure distribution on the cowl has been used to compare our simulated data as shown in figure 5. A fair agreement can be seen between the Cowl pressure distribution, thus, validates the Solver for the internal flow simulation.

In order to converge to an appropriate grid and turbulence model, rigorous grid independence study and the turbulence model study has been performed and already reported in the previously published paper by Sinha et al. [6, 25,35]. Similar grid and turbulence model have been implemented in the current study. Further, to eliminate any kind of deviation in the intrenal air-intake simulations, where the shock pattern are of utmost importance, another set of Grid independence study for the internal flow simulation has been underataken on the data reported by Das and Prasad [36]. Grids of various densities were adopted in order to perform the grid independence study , starting from a coarse grid of appx. 100,000 cells to a fine grid of appx. 200,000 cells. It was observed that on increasing the grid density, the results moved closer to the reported data. With the mesh consisting of 150,000 cells and 200,000 cells showing almost similar results and are in best agreement with the reported data, as can be seen in Figure 6. To accommodate important shock boundary layer interactions, a grid with around 200,000 cells has been adopted for the internal flow simulation.

Thus, from Table 2 and 3 and figure 6, the proper mesh has been generated for both the external simulation on MRDID and the internal simulation on air-intake geometry as shown in Figure 2.

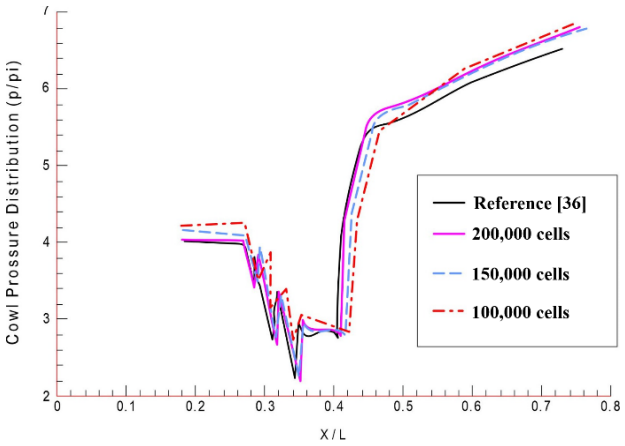

Figure 6. grid Independence test

5. GOVERNING EQUATIONS

For this simulation of k-ω shear stress, a transport turbulence model is used.

$$\mu_t = f\left(\frac{\rho k}{\omega}\right) \tag{1}$$

Turbulent kinetic energy (k) equation:

$$\frac{\partial}{\partial t}(\rho k) + \frac{\partial}{\partial x_i}(\rho k u_i) = \frac{\partial}{\partial x_j}\Gamma_k\left(\frac{\partial k}{\partial x_j}\right) + G_K - y_k \tag{2}$$

Specific dissipation rate (ω) equation:

$$\frac{\partial}{\partial t}(\rho\omega) + \frac{\partial}{\partial x_i}(\rho\omega u_i) = \frac{\partial}{\partial x_j}\Gamma_\omega\left(\frac{\partial \omega}{\partial x_j}\right) + G_\omega - y_\omega \tag{3}$$

The correct equation system that regulates the turbu–lent compressible gas is given in the tensor form below:

Continuity equation:

$$\frac{\partial \rho}{\partial t} + \frac{\partial\left(\rho u_j\right)}{\partial x_j} = 0 \tag{4}$$

Momentum equation:

$$\frac{\partial}{\partial t}(\rho u_t) + \frac{\partial}{\partial x_k}(u_k u_i) + \frac{\partial p}{\partial x_i} = \frac{\partial \tau_{ik}}{\partial x_i} \tag{5}$$

Energy equation:

$$\frac{\partial}{\partial t}(\rho E) + \frac{\partial}{\partial x_k}(\rho u_k H) = -\frac{\partial}{\partial x_k}\left(u_i \tau_{jk}\right) + \frac{\partial q_k}{\partial x_k} \tag{6}$$

where ρ, u_i, p, E, and H denote the density, velocity components, pressure, total energy, and enthalpy, respectively. The term "turbulent shear stress" refers to the amount of force exerted by a moving object., in the term of expression

$$\tau_{ik} = \mu\left(\frac{\partial u_i}{\partial x_k}\right) + \left(\frac{\partial u_k}{\partial x_i}\right) \tag{7}$$

$\mu = \mu_t + \mu_l$ is the total viscosity; μ_t and μ_l being the laminar and turbulent viscosity respectively.

Laminar viscosity calculated from Sutherland law as

$$\mu_i = \mu_{ref}\left(\frac{\partial T}{\partial T_{ref}}\right)^{\frac{3}{2}}\left(\frac{T_{ref}+S}{T+S}\right) \tag{8}$$

where, T is the temperature, T_{ref} and S is the known coefficient.

The stress tensor is expressed as a turbulent vis–cosity (μ_t) function in eddy viscosity models. Based on dimensional analysis, a few variables ((k, ε, ω) are designated as follows:

Turbulent kinetic energy k,

$$k = \overline{u_i u_i} / 2 \tag{9}$$

Turbulent dissipation rate ε,

$$\varepsilon = \overline{\frac{\partial u_i'}{\partial x_i}\left[\frac{\partial'_{u_i}}{\partial x_i} + \frac{\partial u_j'}{\partial x_i}\right]} \tag{10}$$

Specific dissipation rate: $\omega = \frac{\varepsilon}{k}$

The turbulent viscosity u_t is denoted by

$$\mu_t = c_\mu\left(\frac{\rho k^2}{\varepsilon}\right) \tag{11}$$

The heat flux is calculated as,

$$q = -\lambda\frac{\partial T}{\partial x_k} \tag{12}$$

where λ is the thermal conductivity

6. RESULTS AND DISCUSSION

6.1 comparison of conventional air-intake system and MRDID integrated air intake system through mach contours

The steady state simulation for the complete intake geometry with the MRDID and with the conventional intake device was performed with varying intake Mach numbers and a backpressure ratio of 7 bar at 0° angle of attack. For this simulation of the steady state, multiple Mach values were used, including 2, 2.5, 2.8, 3, 3.1, 3.2, 3.5, 4, and 5. The goal of this simulation is to gain an understanding of the starting and unstarting characteristics of a supersonic intake, in addition to the MRD compression rate, and how these features compare to a conventional intake.

Figures 7 and 8 clearly demonstrates that the Normal shock position for both type of intakes is at exterior of the duct, which results in spillage drag. When compared to the conventional intake, the drag value of the MRD integrated intake was found to be significantly higher. It is safe to say that the intake at Mach 2 will continue to be in the unstart condition, and the back pressure value will continue to have an effect on the intake's overall performance.

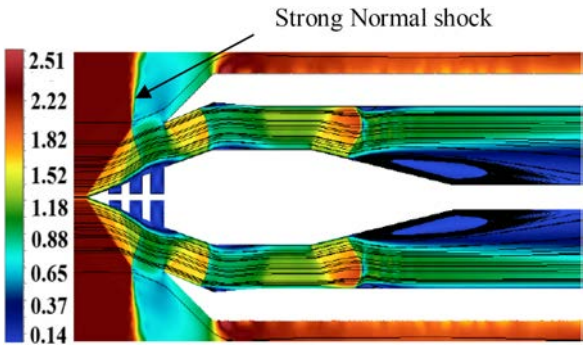

Figure 7. Mach number contours with superimposed streamlines for multi row disk intake at M=2

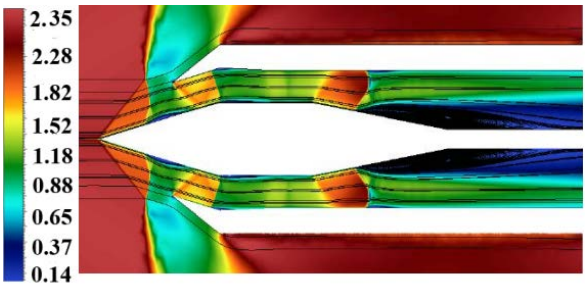

Figure 8. Mach number contours with superimposed streamlines for conventioal intake at M=2

At Mach 2.5 the intake having the low spillage drag compare to Mach 2 condition, we can say that as the intake fly near the design Mach number condition the spillage drag will reduce. For this case backpressure will not vary much. Figure 9 and 10 represents the Mach contour.

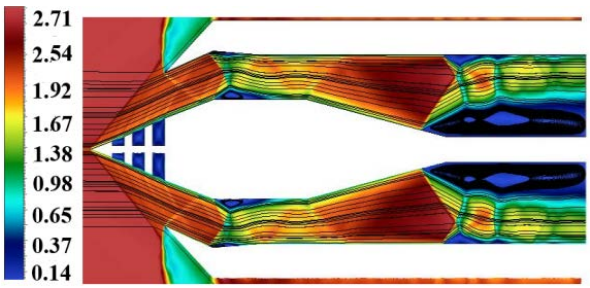

Figure 9. Mach number contours with superimposed streamlines for multi row disk intake at M=2.5

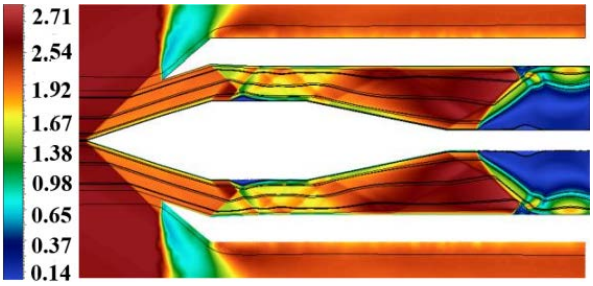

Figure 10. Mach number contours with superimposed streamlines for conventional intake at M=2.5

At Mach 2.8, we are able to observe (figure 11 and 12) that the recirculation zone has begun, and the amount of spillage drag has been significantly reduced; however, the mass capture ratio has not fallen below the figure that is desired.

As we can see from the figure 13 and figure 14 the intake is in started condition, at the Mach 3. As we go

beyond Mach 3, we will get the maximum mass capture ratio, which provides the higher mass flow rate inside the intake and overall engine thrust will increase. Figure 15 has covered the Mach contour upto larger stretch into the air-intake system.

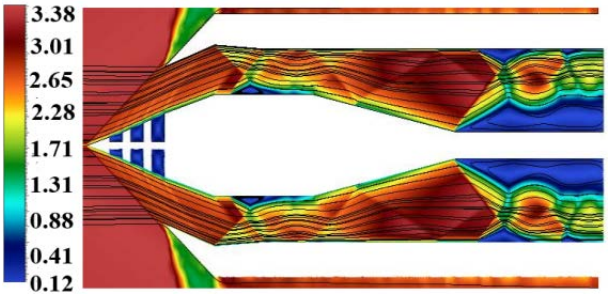

Figure 11. Mach number contours with superimposed streamlines for multi row disk intake at M=2.8

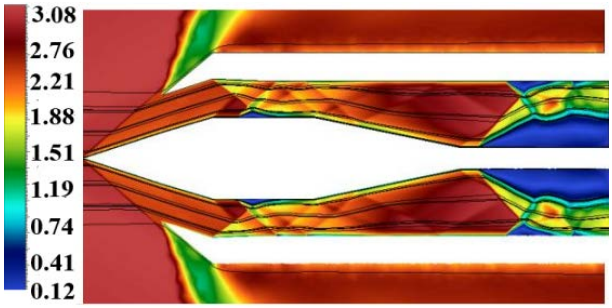

Figure 12. Mach number contours with superimposed streamlines for conventional intake at M=2.8

A detailed re-circulation zone can be seen stretches as we go along the length. It also has multiple blast region formed like a blast train, creating local sonic region near the wall. These blasts offer tremendous thermal challenges to the material of the engine. As the Mach number increases, the flow re-circulation region will expand in size and later it will create a converging-diverging section internal to the air-intake part

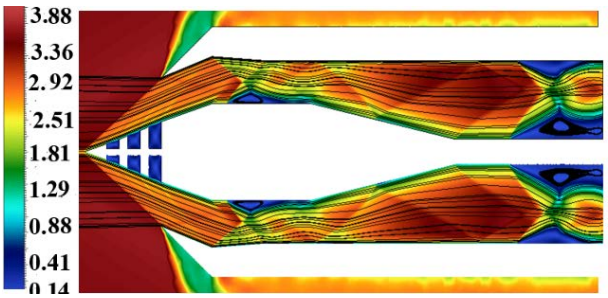

Figure 13. Mach number contours with superimposed streamlines for multi row disk intake at M=3.0

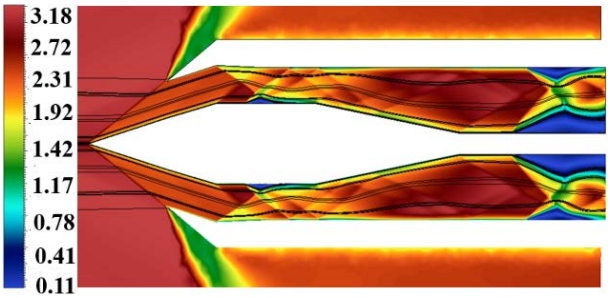

Figure 14. Mach number contours with superimposed streamlines for conventional intake at M=3.0

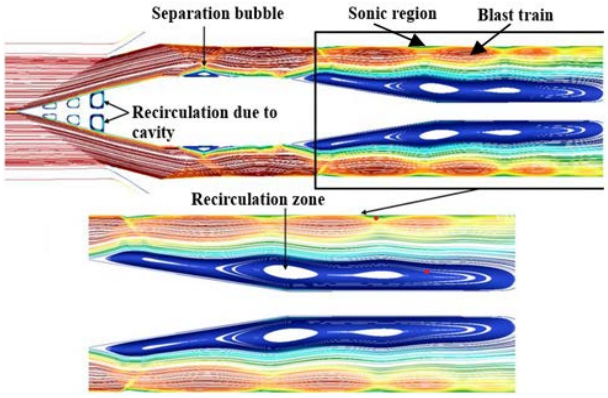

Figure 15. Detailed separation zones developed at Mach 3.0 with MRDID.

Figure 16 to 19 provides the comparison for Mach 3.2 and 3.5. Analysis of the closer ranges of Mach number has helped to understand the gradual development of Blast train, recirculation and further expansion of rec-circulation zone. This paved the way for the analysis on the effect of Back pressure.

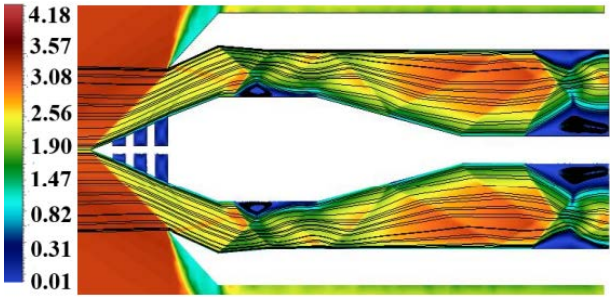

Figure 16. Mach number contours with superimposed streamlines for multi row disk intake at M=3.2

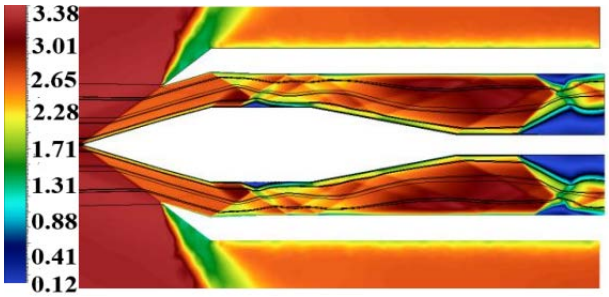

Figure 17. Mach number contours with superimposed streamlines for conventional intake at M=3.2

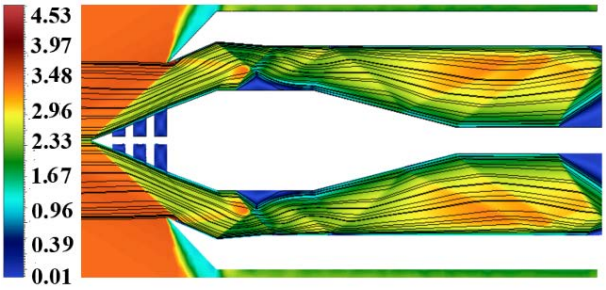

Figure 18. Mach number contours with superimposed streamlines for multi row disk intake at M=3.5

Development of critical intake condition near the Mach 3 has been captured by analyzing multiple cases at Mach 3, 3.2 and 3.5. The figure 18 is also shown in an enlarged view in figure 20. It has depicted large

recirculation zone, sonic zone and blast trains. At Mach 3.5, the local recirculation zone has expanded so much that is forms a vrtual convergent-divergent section.

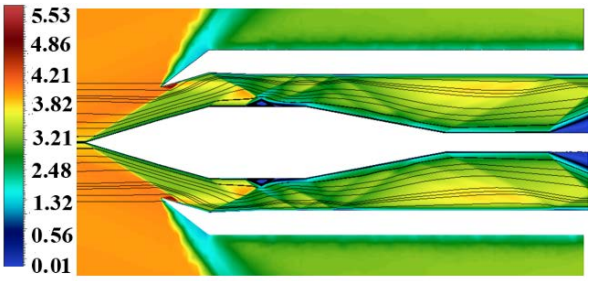

Figure 19. Mach number contours with superimposed streamlines for conventional intake at M=3.5

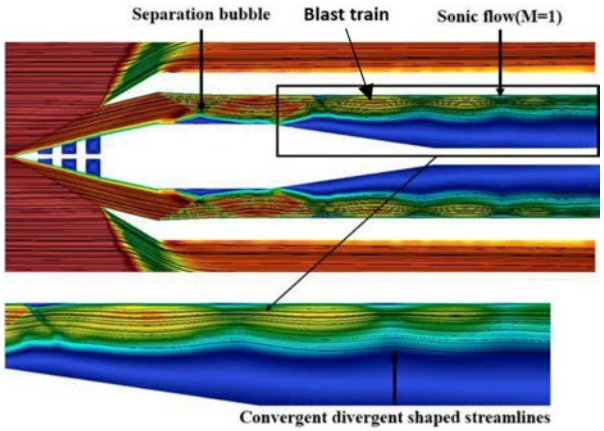

Figure 20. Detailed view of the internal flow development at Mach 3.5

Further contours at Mach 4 and 5 are given below for MRDID integrated intake only in figure 21 and 22.

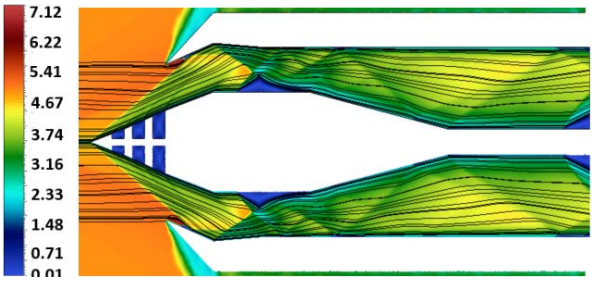

Figure 21. Mach number contours with superimposed streamlines for multi row disk intake at M=4

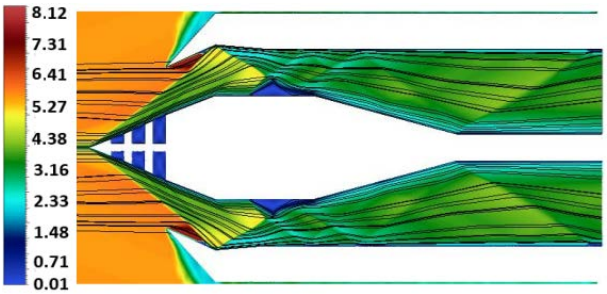

Figure 22. Mach number contours with superimposed streamlines for multi row disk intake at M=5.

6.2 comparison of TPR & MCR for conventional air–intake and the MRDID integrated air intake

The Air-intake is designed to get the maximum pressure recovery and mass capture ratio at designed Mach number, which in this case is 3, as obtained from the Mach contour. The effectiveness of the intake can be characterised by the utilisation of the two important parameters. First, is the Total pressure ratio (TPR). It is determined by taking the average total pressure at the input and comparing it to the average total pressure at the exit. Because the average total pressure at the entrance is always the same, it estimates that the total pressure ratio at the starting and the end of the operation will never change, regardless of the Mach number. For optimal combustion, the intake should have a high total pressure ratio in order to supply air that has been compressed to a higher level. In contrast to what one might have anticipated, the overall pressure loss can be attributed to shock as well as viscous losses. Total pressure ratio, often known as TPR, equals Pt2/Pt1. Higher pressure recovery (closer TPR to 1) results in higher efficiency and more power for the engine.

The second important parameter of an intake that is taken into consideration when determining its efficiency is the capture-area ratio, which is also referred to as the mass-capture ratio (MCR). It is estimated by taking the ratio of the mass flow rate of the air entering the intake and reaching the engine and the mass flow rate of air available in the free stream, typically calculated using the free-stream air density, velocity, and cross-sectional area at the intake. In jet engines, a higher mass capture ratio is desirable for maximizing engine performance and efficiency.

A series of computer simulations were conducted for various Mach numbers for a given Back Pressure. The simulations covered conditions where the Mach number was both less than and greater than the design Mach number ($M < M_{design}$ and $M > M_{design}$), allowing for an investigation of the starting and unstarting characteristics of the intake. Figures 23 and 24 present the computed values for the Total Pressure Ratio (TPR) and mass-averaged Mass Capture Ratio (MCR) for a range of free-stream Mach numbers from 2 to 5, for both conventional and MRDID integrated intake designs.

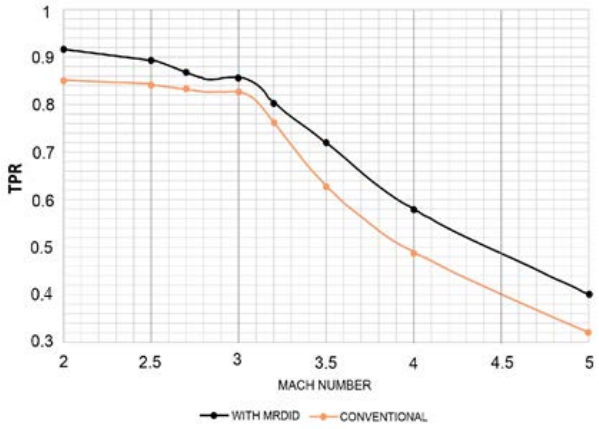

Fig 23. TPR comparison for different Mach number

The data indicate that at lower Mach numbers (M=2 to 2.8), it achieve a higher TPR, but the MCR remains low, suggesting that the intake process has not fully started. As the Mach number increases, there is a natural improvement in MCR which increases from 0.8 to

maximum value of 1 near Mach 3.2. While pressure recovery remains more or less constant in the range of 0.9 to 0.85 before drastically falling beyond Mach 3. Since the Intake has started near Mach 3, so going further we can see that as the Mach number increases to Mach 4 and 5, the MCR and TPR have decreased. The decrease in MCR is mainly due to substantial flow separation caused by shock-boundary layer interactions.

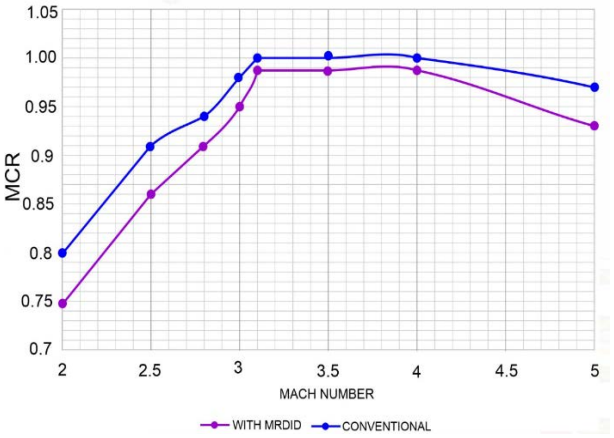

Fig 24. MCR comparison for different Mach number

Based on figure 23 and 24, the MRDID integrated design demonstrates superior performance compared to the conventional design in terms of both TPR and MCR. For the entire range of simulation from Mach 2 to 5, the TPR of the modified design is higher by almost 5-10% due to the inclusion of disks that increase flow compression and energy, resulting in a rise in static pressure. The graph also shows that even under off-design conditions, the modified intake demonstrates better performance than conventional intake. Though near Mach 3, the TPR and MCR for both the intakes have come closer but as the Mach number goes below or above Mach 3, the significant peformance loss in conventional air intake system can be seen as compared to MRDID integrated air intake.

6.3 EFFECT OF ANGLE OF ATTACK ON THE PERFORMANCE OF MRDID INTEGRATED AIR INTAKE SYSTEM

In the previous section we have seen the comparison of Conventional air-intake system and the MRDID integrated air-intake system. So, we have established the advantage of the later over the former. In this segment, the purpose is to develop the flow physics inside the air-intake system when the the angle of attack increases further. No comparison has been done with conve–ntional air-intake system, focus is totally on evaluating the performance of the MRDID integrated system.

The study investigates the performance of an intake operating under supersonic flow conditions, with a Mach number of 3 and a back pressure ratio of 7 bars. Simulations were conducted at various angles of attack (AoA), specifically 1°, 2.5°, 4°, 5°, 6°, 8°, and 10°, to evaluate the effect of AoA on total pressure recovery, a critical parameter for intake efficiency.

Following figure 25-27 shows the change in flow features over the angle of attack of 1°, 4° and 10°.

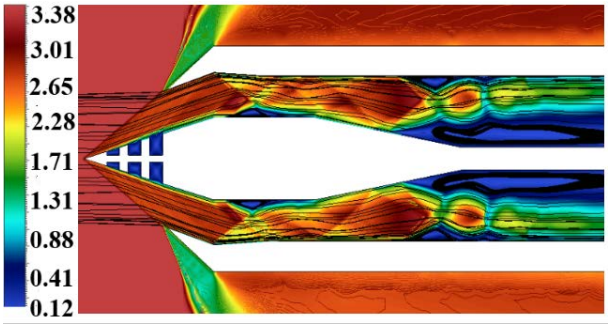

Figure 25 (a). Mach contour at 1° AoA

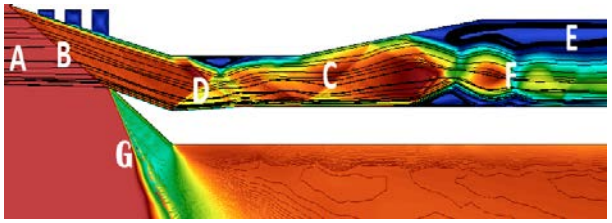

Figure 25 (b) Enlarged view of the lower symmetrical section

Enlarged view of the above image has been provided as Figure 25 (b) for better understanding and they have been marked as per the region of interest.

Key regions of interest in the figure 25:

(A) **Supersonic Freestream Flow Region**: The red area at the intake (left side) represents a supersonic freestream with a Mach number around 3.0. This region shows the undisturbed flow approaching the intake.

(B) **Oblique Shock Waves:** The slanted lines with a sharp change in Mach number (from red to green/yellow) inside the intake indicate the presence of oblique shock waves. These shocks occur as the supersonic flow encounters a change in the geometry, causing a drop in Mach number and an increase in static pressure and temperature. Multiple oblique shocks are visible, suggesting staged compression.

(C) **Internal Shock Interaction Region:** The complex patterns of alternating colors (red, yellow, green, blue) inside the intake show areas where oblique shocks interact with one another or reflect off the walls. These interactions can lead to additional compression and further losses.

(D) **Boundary Layer and Flow Separation:** Near the walls of the intake, particularly where the color transitions gradually (e.g., from green/yellow to blue), there may be indications of a developing boundary layer. Regions where the contour lines are close together and the Mach number decreases rapidly may suggest boundary layer thickening or separation due to shock-boundary layer interaction.

(E) **Subsonic Flow Regions:** The blue and dark blue areas further downstream inside the intake suggest regions where the flow has decelerated to subsonic speeds (Mach number below 1.0). This transition is due to normal shocks and excessive losses due to shock interactions and boundary layer separation, leading to flow recirculation.

(F) **Normal Shock Wave or Terminal Shock:** The abrupt change from warmer (yellow/green) to

cooler colors (blue) in the middle-to-end of the intake likely represents a normal shock wave or terminal shock, which decelerates the supersonic flow to subsonic speeds. This is a critical region for pressure recovery in the intake.

(G)**External Flow and Shock Interactions:** On the exterior surfaces of the intake (near the top left and bottom left corners), the sudden change in colors suggests external shock interactions or the formation of a detached bow shock in front of the intake. These shocks can cause flow deflection and additional drag.

Figure 26 provides the Mach contour for AoA of 4°. The upper symmetrical part of the Air-intake or the leeward part shows the flow separation from the top wall and the weaker oblique shock, whereas the lower symmetrical part or the wind ward side shows stronger oblique shock from the tip to the cowl tip and flow separation from the lower wall.

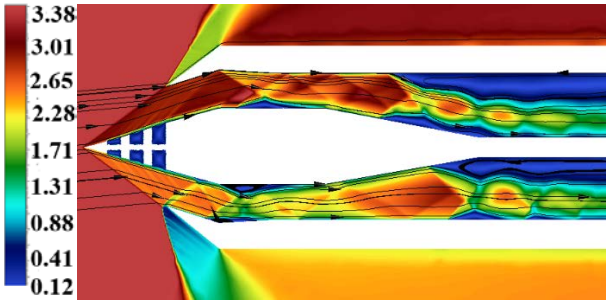

Figure 26. Mach contour at 4° AoA

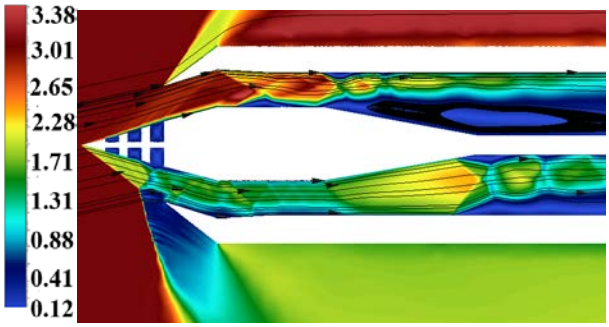

Figure 27. Mach contour at 10° AoA

Figure 27 shows the air-intake subjected to extreme 10° AoA. Strong shock at the cowl tip shows strong external flow and oblique shock interaction at region G marked in figure 24 (b) of the wind ward side, huge flow losses and additional drag at the wind ward side. It also indicates stronger Normal shock inside the Air-intake geometry, evident by large subsonic region downstream.. Thus it indicates that there will be loss in performance as measured by TPR for different angle of attacks.

TPR vs AoA as shown in figure 28, indicates that total pressure recovery increases with the angle of attack up to 6°. This trend suggests that at lower angles of attack, the intake effectively manages the oblique shock waves and maintains favorable boundary layer behavior, leading to minimal flow separation and efficient air intake. However, at higher angles of attack, specifically 8° and 10°, there is a noticeable decline in total pressure recovery. This reduction is likely due to flow separation, intensified shock-induced losses, and the formation of stronger oblique or normal shocks, which result in greater total pressure loss.

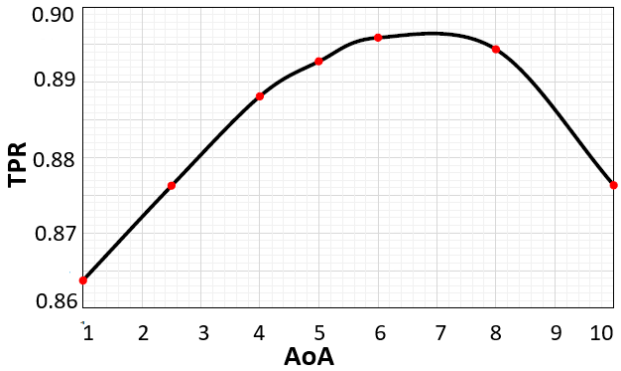

Figure 28. TPR vs AoA

The initial increase in total pressure recovery at lower angles of attack (up to 6°) could be attributed to the alignment of the airflow with the intake, which minimizes spillage and maintains aerodynamic efficiency. Beyond 6°, the performance deterioration can be explained by the onset of adverse aerodynamic effects, such as shock-boundary layer interactions and separation phenomena, which contribute to increased entropy generation and energy losses.

7. CONCLUSION

Air-intake is an essential part of a high speed engine and its design impacts the overall performance of the engine. Computational studies of the 2D supersonic air-intake at different Mach number ranging from 2 to 5 and at different AoA ranging from 1° to 10°is presented in this paper. In-house algorithm and code is fed on commercial CFD software, coupled with density-based Reynolds-averaged Navier-Stokes equations (RANS) equations, and further solved with a k-ω SST turbulence model. The computed Mach contour distribution and intake performance parameters (TPR and MCR) comprehensively discussed for Conventional air-intake system and MRDID integrated air–intake system. The MCR & TPR determines the free-stream Mach number at which intake unstarting and starting occurs.

Overall Conclusion can be broken down based on the following parameters:

1. **Flow Visualization**:

.

- The Mach number distribution indicates significant reduction in shock intensity, especially in the presence of the MRDID, which enhances the overall efficiency of the system.
- From the contour plot, the presence of MRDID demonstrates better performance, as it maintains higher Mach numbers at critical sections of the nozzle. This results in improved flow uniformity, reducing losses.

2. **TPR vs Mach Number analysis**

- The graph indicates that total pressure recovery (TPR) decreases as the Mach number increases.

- However, the presence of MRDID(black curve) helps in maintaining a higher TPR compared to the system without it (orange curve), especially at higher Mach numbers. This indicates better overall system efficiency and reduced losses in systems with MRDID.

3. MCR vs Mach Number

- Around Mach 2.5, the performance of the air-intake with MRDID configuration improves sharply, surpassing the conventional system around Mach 3. This suggests that MRDID becomes more effective as speed increases in this range.
- At higher Mach numbers, both configurations exhibit a gradual decline in MCR. However, the "With MRDID" system maintains a slight advantage over the conventional design, indicating it is more effective at higher speeds.

4. TPR vs AoA

- Up to an AoA of 6 degrees, total pressure recovery improves. This likely happens because the intake can handle the oblique shocks and the boundary layer behavior remains attached or minimally separated, maintaining efficient air intake.
- At higher angles of attack (8 and 10 degrees), total pressure recovery decreases. This decline is likely due to flow separation, increased shock losses, or the formation of stronger oblique or even normal shocks in the intake, which lead to greater energy losses and reduced efficiency.

These findings suggest that the intake design has best operating range of Mach 3-3.2 and is optimized for angles of attack up to approximately 6°, beyond which performance degradation becomes significant. The decline in total pressure recovery at higher angles of attack indicates that the intake may be susceptible to shock-induced separation or other aerodynamic inefficiencies under these conditions. To mitigate this performance loss, further research could explore design modifications, such as adjusting the intake geometry, implementing boundary layer control techniques, or incorporating shock management mechanisms to enhance pressure recovery at higher angles of attack.

Based on the TPR and MCR graphs we have obtained almost 5-10% modifications with the implementation of the MRDID over conventional intake. These values are significant as we have used only a scaled miniature model for the simulations. In case of full fledged air-intake model and for the full 3D case, these differences will further widen and MRDID can be a very efficient improvement over conventional intakes.

ACKNOWLEDGMENT

Authors would like to thank all the faculty and staff members of Amity Institute of Aerospace Engineering, who provided valuable feedback during this research.

REFERENCES

[1] Ogura, S. et al: Experimental study of high-speed air intake performance by side clearance, Aerospace Science and Technology, Vol. 123, April 2022.

[2] Borovikov A., Gavriliouk V., Gilevich I., Duganov V., Khokhlov A. and Stepanov V.: Gas dynamic design of supersonic and hypersonic airframe integrated inlets and nozzles. AIAA Paper No. 96-4549, 1996.

[3] Merchant, V, and Radhakrishnan, J.: Design and Optimization of Supersonic Intake, IOP Conference Series, Materials Science and Engineering, 225-012298, 2017.

[4] Laruelle, G.: Air Intakes: Role, Constraints and Design, ICAS CONGRESS, 2002.

[5] El-Sayed, A.F. and Emeara, M.S.: Aero-Engines Intake: A Review and Case Study, Journal of Robotics and Mechanical Engineering Research, Vol. 1, Issue-3. pp. 35-42, 2016.

[6] Sinha, J., Singh, S., Prakash, O. and Panchal, D.: Design Optimization of a Multi Row Disk Inlet Device with an Optimum Nose Cone Angle, FME Transactions, Vol. 51, No. 1, pp. 23-30, 2023.

[7] Seddon, J. and Goldsmith, E.L.: Intake Aerodynamics, 2nd Edition, Blackwell Science 1999.

[8] Cakir, B.O., Ispir, A.C. and Saracoglu, B.H.: Reduced order design and investigation of intakes for high speed propulsion systems,, Acta Astronautica, Vol. 199, 2022, pp. 259-276.

[9] Kojima, T., Sato, T., Sawai, S. and Tanatsugu, N., 2004. Experimental study on restart control of a supersonic air-breathing engine. Journal of propulsion and power, Vol. 20, No. 2, pp.273-279, 2004.

[10] Hoheisel, H.: Aerodynamic aspects of engine-aircraft integration of transport aircraft, Aerosp. Sci. Technol., 1 (7) (1997), pp. 475-487.

[11] Babinsky, H., Li, Y. and Pitt Ford, C.W.: Microramp control of supersonic oblique shockwave/boundary-layer interactions, AIAA Journal, Vol. 47, No. 3, pp. 668–675, 2009.

[12] Soltani, M.R, Abedi, M., Askari, R. and Sepahi, Y.J.: Axisymmetric and three-dimensional flow simulation of a mixed compression supersonic air intake, 13th International Conference on Heat Transfer, Fluid Mechanics and Thermodynamics, pp. 886-891, 2017.

[13] Askari, R., Soltani, M.R., Mostoufi, K., Khajeh Fard, A. and Abedi, M.: Angle of attack investigations on the performance of a diverterless supersonic inlet, Journal of Applied Fluid Mechanics, Vol. 12, No. 6, pp.2017-2030, 2019.

[14] Noftz, M.E., Jewell, J.S., Bustard, A., Juliano, T.J. and Bisek, N.J.: Investigation of an Inward-Turning Intake at Negative Angle of Attack, AIAA Aviation Forum and Ascend 2024, AIAA 2024-3976, 2024.

[15] Krushnarao Kotteda, V.M. and Mittal, S.: Flow in a Y-intake at supersonic speeds. Journal of Propulsion and Power, *Vol. 32*, No.1, pp.171-187, 2016.

[16] Fujii, M., Ogura, S., Sato, T., Taguchi, H., Hashimoto, A. and Takahashi, T.: Effect of angle of attack on the performance of the supersonic intake for High Mach Integrated Control Experiment (HIMICO), Aerospace Science and Technology, Vol. 127, pp. 107687, 2022.

[17] Trapier, S., Duveau, P. and Deck, S.: Experimental Study of supersonic inlet buzz, AIAA Journal, Vol. 44, No. 10, pp.2354-2365, 2006.

[18] Lee, H.J. and Jeung, I.S., 2009, April. Experimental and numerical investigation on the supersonic inlet buzz with angle of attack, Shock Waves, Volume 2, pp. 1111-1116, 2009.

[19] Chudhary, P.K.: Effect of Back Pressure on the Performance of Supersonic Intake, IJERT, Vol. 10, Issue-7, pp. 500-504, 2021.

[20] Van Wie, D., Kwok, F. and Walsh, R., 1996, July. Starting characteristics of supersonic inlets, AIAA Paper 96-2914.

[21] Namkoung, H.J., Hong, W., Kim, J.M., Yi, J. and Kim, C.: Effects of angles of attack and throttling conditions on Supersonic Inlet Buzz, Int'l J. of Aeronautical & Space Sci. Vol. 13, No. 3, pp. 296–305, 2012.

[22] Yu, K., Xu, J., Li, R., Liu, S. and Zhang, X.: Experimental exploration of inlet start process in continuously variable Mach number wind tunnel, Aerospace Science and Technology, Vol. 79, pp.75-84. 2018

[23] Kobayashi, H., Maru, Y. Hongoh, M., Takeuchi, S., Okai, K. and Kojima, T.: Study on variable-shape supersonic inlets and missiles with MRD device, Acta Astronautica Vol. 61, pp. 978 –988. 2007.

[24] Kobayashi, H., Kojima, T., Okai, K. and Maru, Y.: Study of Supersonic Cavity Flow in Advanced Variable Geometry Inlet, *55th International Astronautical Congress* Vancouver, Canada. 2004.

[25] Sinha, J., Arora, K., Prakash, O., Bandopadhyay S., Saha, P. and Bhattacharya, A.: Analysis of multi row disk inlet device in supersonic flow condition, *21st Annual CFD Symposium*, August 2019, Bangalore, India.

[26] Emami, S. & Trexler, C.: A. Experimental investigation of inlet combustor – isolators for a dual mode scramjet at a Mach number of 4. NASA Technical Report No. NASA TP3502, May 1995.

[27] Tam, C. J., Orkis, P. D., and Disimile, P. J.:Algebric turbulence model simulations of supersonic open cavity flow physics. AIAA Journal, Vol. 34 No. 11, pp.2255-2260, 1996.

[28] Sanal Kumar, V.R., Sankar, V., Nichith, C., Saravanan, V., et al.: A closed-form analytical model for predicting 3D boundary layer displacement thickness for the validation of viscous flow solvers, AIP Advances, Vol. 8, Issue: 02, Article No. 025315, 2018.

[29] Gholap, T.B., Salokhe, R.V., Ghadage, G.V., Mane S.V., and Sahoo, D.: Aerodynamic Analysis of an AK-47 Bullet Moving at Mach 2.0 in close proximity to the Ground, FME Transactions, Vol. 50, No. 2, pp. 369-381, 2022.

[30] Taha, A.A., Tiwari, S.N., and Mohieldin, T.O.: Validation of fluent CFD code in supersonic flow fields, 15th AIAA Computational Fluid Dynamics Conference, 2001, Anaheim CA, AIAA 2001-2637.

[31] Tembhurnikar, P.V., Jadhav, A.T. and Sahoo, D.: Effect of Intermediate Aerodisk Mounted Sharp Tip Spike on the Drag Reduction over a Hemispherical Body at Mach 2.0, FME Transactions, Vol. 48, pp. 779-786, 2020.

[32] Milićev, SS.: An Experimental Study of the Influence of Spike in Supersonic and Transonic Flows Past a Hemispheric Body, FME Transactions, Vol. 50, No. 1, PP. pp. 24-31, 2022.

[33] Damljanović, D., Vuković, D., Ocokoljić, G., Rašuo, B.: Convergence of Transonic Wind Tunnel Test Results of the AGARD-B Standard Model, FME Transactions, Vol. 48, No. 4, pp. 761-769, 2020.

[34] Damljanović, D., Vuković, Đ., Ocokoljić, G., Ilić B., and Rašuo, B.: Wind Tunnel Testing of ONERAM, AGARD-B and HB-2 Standard Models at Off-Design Conditions, Aerospace, Vol. 8, No. 10, 275, 22 Sep. 2021.

[35] Sinha, J., Singh, S., Prakash, O. and Panchal, D.: Passive flow modification over the Supersonic and the Hypersonic air-intake system using Bleed**,** FME Transactions, Vol. 51, No. 2, pp. 329-337, 2023.

[36] Das, S. and Prasad, J.K.: Starting characteristics of a rectangular supersonic air-intake with cowl deflection, The Aeronautical Journal, Vol. 114, No. 1153, pp. 177–89, 2010.

NOMENCLATURE

MRD	Multi Row Disk
RANS	Reynolds-Averaged Navier-Stokes
MRDID	Multi Row Disk Inlet Device
$k-\omega$ *SST*	$k-\omega$ shear stress transport
TPR	Total pressure ratio
MCR	Mass capture ratio
AoA	Angle of attack
θ	shock angle
β	deflection angle
M	Mach number
x/L	Ratio of wetted length and the intake throat height
C_D	Drag coefficient
P	Pressure
Pinf	Free stream pressure
Pi	Free stream pressure

АНАЛИЗА ДИЗАЈНА НАДЗВУЧНОГ УСИСНИКА ЗА УРЕЂАЈ ЗА УСИСАВАЊЕ ВИШЕРЕДНИХ ДИСКОВА ПОД РАЗЛИЧИТИМ МАХОВИМ БРОЈЕВИМА И НАПАДНИМ УГЛОМ

Ј. Синха, С. Синг, О. Пракаш, Д. Панцал

Ово истраживање истражује перформансе МРД дизајна усисника за суперсоничне авионске моторе, фокусирајући се на његово понашање под различитим Маховим бројевима и нападним угловима. Користећи стабилне, дводимензионалне РАНС симулације са к-ω ССТ моделом турбуленције, студија пореди унос МРД са конвенционалним дизајном усисника. Симулације су спроведене у распону Махових бројева од 2,0 до 5,0 под нападним углом од 0° до 10°. Резултати откривају да МРД унос постиже оптимални однос захвата масе и укупни опоравак притиска близу пројектованог Маховог броја од 3, значајно надма–шујући конвенционалне уносе у смислу ефикас–ности и стабилности. Анализа такође наглашава утицај раздвајања протока на перформансе усисника, посебно при ниским и високим Маховим бројевима. Штавише, студија истражује ефекте различитих углова напада, показујући повећање укупног опоравка притиска до 6°, након чега перформансе почињу да опадају. Ови налази пружају вредан увид у аеродинамичку оптимизацију надзвучних усисника, нудећи потенцијална побољшања у дизајну и раду авиона велике брзине.